Conjugated Polymer-Mediated Polymorphism of High Performance, Small-Molecule Organic Semiconductor with Tuned Intermolecular Interactions, Enhanced Long-Range Order and Charge Tran...

ARTICLE *in* CHEMISTRY OF MATERIALS · OCTOBER 2013

Impact Factor: 8.35 · DOI: 10.1021/cm403039y

CHEMISTRY OF MATERIALS

Article

pubs.acs.org/cm

Conjugated Polymer-Mediated Polymorphism of a High Performance, Small-Molecule Organic Semiconductor with Tuned Intermolecular Interactions, Enhanced Long-Range Order, and Charge Transport

Jihua Chen,*[,†] Ming Shao,[†] Kai Xiao,[†] Zhengran He,[‡] Dawen Li,[‡] Bradley S. Lokitz,[†] Dale K. Hensley,[†] S. Michael Kilbey, II,[§] John E. Anthony,[∥] Jong K. Keum,[⊥] Adam J. Rondinone,[†] Wen-Ya Lee,[#] Sanghyun Hong,[#] and Zhenan Bao*[,#]

[†]Center for Nanophase Materials Sciences, Oak Ridge National Laboratory, Oak Ridge, Tennessee 37831, United States

[‡]Department of Electrical and Computer Engineering, Center for Materials For Information Technology, University of Alabama, Tuscaloosa, Alabama 35487, United States

[§]Department of Chemistry, University of Tennessee, Knoxville, Tennessee 37996, United States

[∥]Department of Chemistry, University of Kentucky, Lexington, Kentucky 40506, United States

[⊥]Neutron Scattering Science Division, Oak Ridge National Laboratory, Oak Ridge, Tennessee 37831, United States

[#]Department of Chemical Engineering, Stanford University, Stanford, California 94305, United States

Supporting Information

ABSTRACT: We use 6,13-bis(triisopropylsilylethynyl)pentacene as a model small molecule organic semiconductor and two conjugated polymer additives to demonstrate conjugated polymer-mediated polymorphism of a small molecule organic semiconductor for the first time. The conjugated polymer additives, used with a slow solution crystallization approach, yield crystal structures that are not accessible by nonconjugated polymer additives and impart excellent long-range order. In both of the small molecule semiconductor/conjugated polymer blends studied here, previously unreported polymorphs of a small molecule semiconductor have been identified which also leads to improved charge transport in the absence of external alignment. These results open up a new exciting avenue to manipulate unit cell structure, long-range order, and charge transport of high performance, solution-processed, small molecule organic semiconductors.

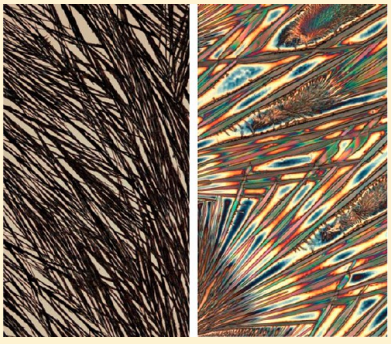

KEYWORDS: *solution crystallization, small molecule organic semiconductor, conjugated polymers, crystal structure, thin film polymorphism, charge transport*

INTRODUCTION

Polymorphism results from the ability of a solid material to organize and pack into two or more unit cell structures in its crystalline forms. Polymorphism plays critical roles in the properties and performance of a variety of crystalline materials, including organic and molecular crystals,[1] and Nature displays impressive control of polymorphism in inorganic crystals. For example, organisms are able to exert strikingly precise in vivo control of the polymorphs of their precipitated calcium carbonate crystals (calcite or aragonite), creating at a given location using self-synthesized biological macromolecules.[2] Belcher et al. demonstrated that soluble polyanionic proteins extracted from an abalone shell can abruptly switch the polymorphs of calcium carbonate during crystallization.[3] Matzger and co-workers used a library of insoluble synthetic polymer additives to develop the so-called "polymer heteronuclei-induced crystallization" method, which largely facilitates polymorph selection of solution-grown organic single crystals, especially pharmaceutical crystals.[4] It is hypothesized that the initial aggregated cluster formation and kinetics of heterogeneous nucleation are decisive in polymorphism, which can be affected by the specific intermolecular interactions between the nuclei in forming and the biological or synthetic polymer additives.[1,2,4]

The crystallization and polymorphism of small molecule organic semiconductors are of paramount importance in determining the microstructure and charge transport of various organic electronic devices such as organic thin film transistors (OTFTs), solar cells, and sensors.[5,6] The small molecule organic semiconductor 6,13-bis(triisopropylsilylethynyl)-pentacene (TIPS-pentacene, or TP) has attracted intense scientific attention since its discovery because of its air stability,

Received: August 7, 2013
Revised: October 8, 2013
Published: October 8, 2013

Scheme 1. Molecular Structures of the Small Molecule Organic Semiconductor TP and the Two Conjugated Polymer Additives, P3HT and PnBT-RRa

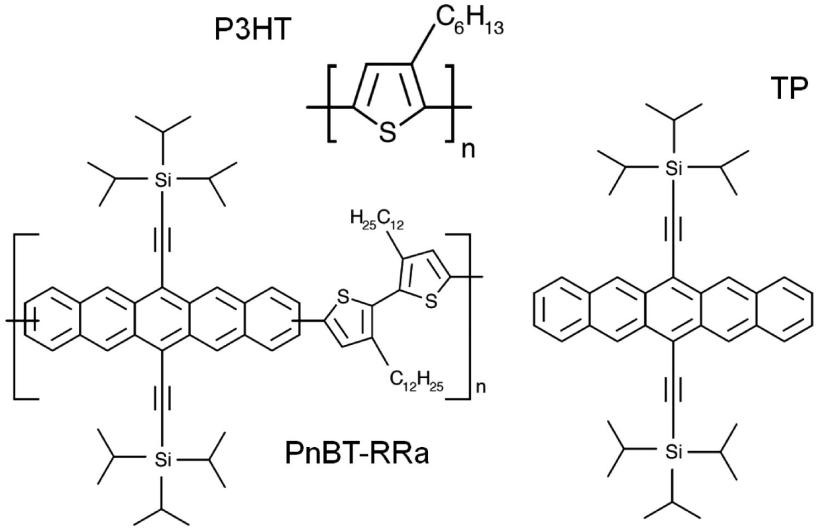

versatile solvent choices, and high hole mobility (up to 1.4 cm^2 V^{-1} s^{-1} without solution shear, and up to 4.6 cm^2 V^{-1} s^{-1} with optimized solution shear).[6−12] Various approaches, including additives and external field-induced alignment methods have been adopted to manipulate the crystallization of TP, to optimize its charge transport within the resultant crystalline thin films. For example, Giri et al. used a solution shear method to apply lattice strain on the TP unit cell, reducing the $\pi-\pi$ stacking distance from 3.33 Å to 3.08 Å, and increasing the hole mobility of TP by 5−6 fold.[6] Other external alignment methods applied to control the crystallization of TP include substrate tilting,[13] air navigation,[9,14,15] dip-coating,[8] and scanning corona-discharge coating.[16] In the additive approaches, nonconjugated polymers (such as poly(α-methylstyrene))[10,17] and insulating SiO_2 nanoparticles[18] were used to manipulate the vertical and lateral phase separation in the TP-based blends, while poor solvents were often introduced to yield solution-processed TP single crystals.[11,19] Thin films of TP-based blends with conjugated polymer additive poly[bis(4-phenyl)(2,4,6-trimethylphenyl)amine] (PTAA) were previously fabricated with a spin-coating method, yielding spherulitic TP crystals on the top surface of the blend film.[17] It is noted that no TP unit cell changes were reported for most of these external alignment and additive approaches, except in the case of the solution shear method.[6] Slow solution crystallization of small molecule organic semiconductors with conjugated polymer additives have not been reported previously to the best of our knowledge. In addition, structural similarity between the additive and small molecule organic semiconductor are largely underexplored with regard to their effects on resultant crystal structures and long-range order.

Using TP as a model small molecule semiconductor and two conjugated polymers with distinctively different structural similarity to TP, we demonstrate for the first time, "conjugated polymer-mediated polymorphism" of small molecule organic semiconductor for the first time, which leads to excellent long-range order and improved charge transport in the absence of any external alignment techniques. The combination of conjugated polymer additives and a slow solution crystallization approach leads to crystal structures that are distinctly different from the ones achieved with nonconjugated polymer additives or external-field induced alignment. Grazing incidence X-ray diffraction (GIXRD), selected area electron diffraction (SAED), energy-filtered TEM (EFTEM), SEM, and polarized optical microscopy are used to examine the thin film crystal structure, spatial distribution of individual components, and unit cell parameters of TP polymorphs resulting from conjugated polymer-mediated solution crystallization. In addition, UV−vis absorption, crystallinity, and water contact angle measurements consistently show strong dependence on the molecular structure of the conjugated polymer additive in the TP blends.

EXPERIMENTAL SECTION

Materials. TP and regiorandom pentacene−bithiophene polymer (PnBT-RRa) (M_n = 20 000−30 000 g·mol^{-1}) are synthesized based on previously published procedures.[7,20] Poly(3-hexylthiophene) (P3HT) is purchased from Rieke Metals (BASF Sepiolid P200, M_n ∼ 20 000 g mol^{-1} by Gel Permeation Chromatography, or GPC).

Film Formation. TP and polymer powder (1:1 by weight) are dissolved into anhydrous toluene solvent at a total-solids concentration of 0.5% wt. Drop-casting of pristine TP or TP/polymer blend solution is performed in a covered, solvent-vapor-rich, glass Petri dish at ambient conditions, and a typical slow solution crystallization process will take 0.5−1 h.

Transmission Electron Microscopy and Electron Diffraction Simulation. Electron diffraction and TEM are conducted in a Zeiss Libra 120 at 120 kV with an in-column energy (Omega) filter. Electron energy loss spectra results are collected before using the conventional three-window method for elemental mapping, with an energy window of 20 eV. Electron diffraction experiments are performed with an emission current of ∼5 × 10^{-6} A and a selected area aperture of ∼1 μm in diameter. The electron diffraction patterns are calibrated against Al(111) standard (0.234 nm). A minimum electron dose condition was used, and the selected area electron diffraction patterns were obtained with an exposure time of 0.5 s, which was at least 3−5 times shorter than the (experimentally observed) critical exposure time required to severely damage the crystalline lattices. Simulated unit cell views and electron diffraction patterns are generated using CrystalMaker8.2, SingleCrystal 1.5, and Mercury2.3 (www.ccdc.cam.ac.uk/mercury/).

Organic Thin Film Transistors. Bottom-gate, top-contact transistors are fabricated on heavily doped n-type Si substrate with 300-nm-thick thermal oxide layer and phenyltrichlorosilane (PTS) surface treatment.[6] After active layer deposition (slow solution crystallization), the 50-nm-thick gold electrode is vacuum evaporated

dx.doi.org/10.1021/cm403039y | Chem. Mater. 2013, 25, 4378−4386

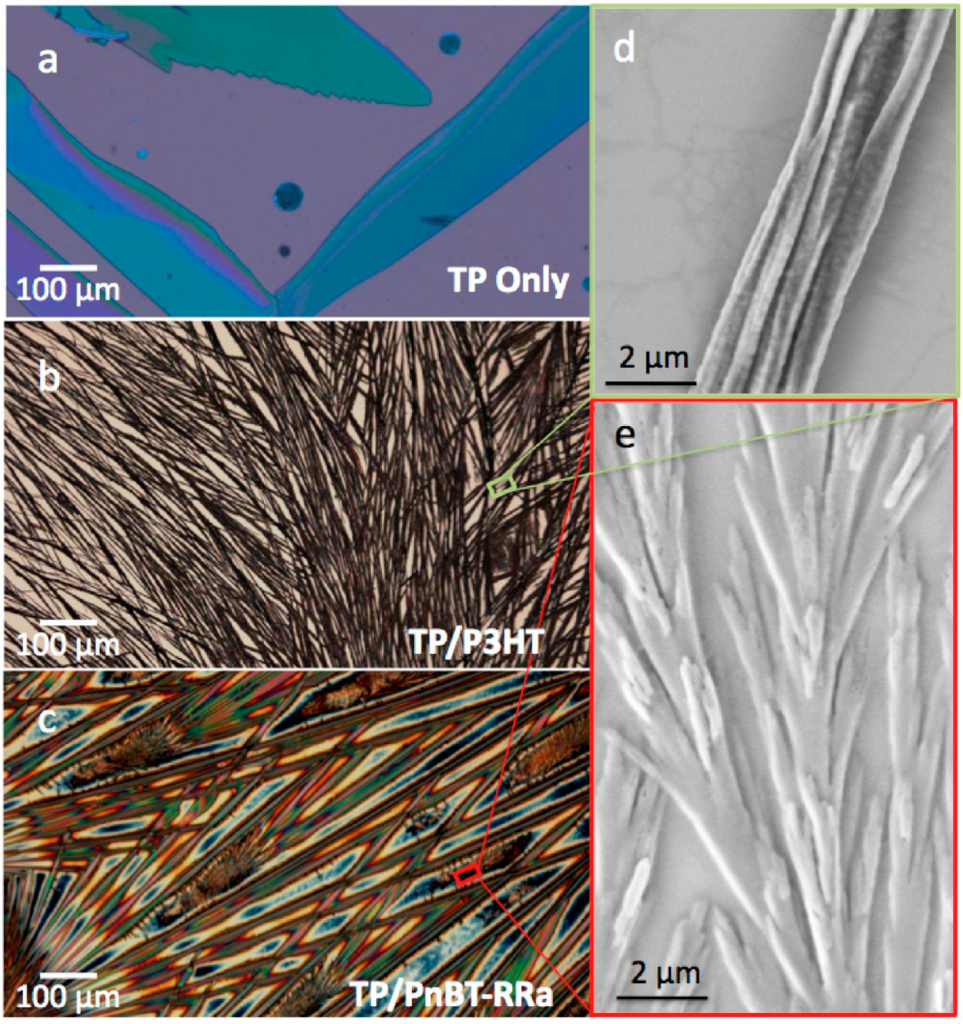

Figure 1. Optical micrographs of the three TP-based thin films slowly crystallized from dilute toluene solutions on silicon wafers: (a) pristine TP films have randomly oriented crystals and large gaps, while (b) TP/P3HT and (c) TP/PnBT-RRa blends show excellent long-range order. An SEM image of the TP/P3HT wires is shown in panel d, and an SEM of the small-grain area of the TP/PnBT-RRa blend is shown in panel e. Red and green boxes indicate the typical locations for SEM images.

through a shadow mask in a thermal evaporator at a high vacuum of 10^{-7} Torr with a deposition rate of 0.5−1 Å s^{-1}. Electrical measurements of OTFTs are carried out in ambient environment with a Keithley 4200 semiconductor analyzer.

Other Thin Film Characterization. Water contact angle measurements are performed with a Kruss DSA30. For each measurement, 3 μL of deionized water is used, along with a sessile fitting. GIXRD experiments are performed in a Philips X'Pert diffractometer with Cu Kα source (wavelength of 1.54 Å). A fixed grazing incidence angle is used, combined with a line scan detector in the incidence plane.

RESULTS AND DISCUSSION

Scheme 1 shows the molecular structure of TP and the two conjugated polymer additives: regiorandom 6,13-bis-(triisopropylsilylethynyl)pentacene-bidodecylthiophene copolymer (regiorandom pentacene-bithiophene, or PnBT-RRa),[20] and poly(3-hexylthiophene) (P3HT, from Rieke Metals: BASF Sepiolid P200). The synthesis and characterization of PnBT-RRa has been reported previously.[20] Figure 1a−c shows optical micrographs of slowly crystallized TP, TP/P3HT, and TP/PnBT-RRa blends (1:1 by weight), respectively, formed on silicon wafers by drop-casting from dilute anhydrous toluene solution (0.5 wt %) in a solvent-vapor-rich environment without the usage of any external alignment techniques. The pristine TP film is poorly covered, having large needle-shaped crystals (having widths on the order of 100 μm and lengths up to millimeters) with essentially random crystal orientations *in the film plane*. TP/P3HT 1:1 blend (by weight) forms grasslike, curved microwire bundles with improved long-range order, while TP/PnBT-RRa 1:1 blend (by weight) crystallizes into a "woven" straight needle pattern with significantly enhanced film coverage and long-range order (up to centimeters). The surface coverage of the TP/PnBT-RRa blend is significantly better than that of TP/P3HT, as indicated by their color-gradient appearance throughout the film surface unlike the "clean" uncovered areas (wafer surface) in TP/P3HT blends. Low-voltage (3 kV) SEM images of TP/P3HT microwires and the small grain area of TP/PnBT-RRa blends are presented in Figure 1d and 1e, respectively, both showing microstructures that are not accessible by crystallization of pristine TP films or TP/nonconjugated polymer blends.[10,21] Nonconjugated polymer additive is known to induce vertical phase separation in TP/polymer blend at an appropriate blend ratio, without changing the crystal habits of the small molecule organic semiconductor.[10] GIXRD of those three films (Figure 2) shows dominating (001)-type reflections of TP crystals, and the *d*

dx.doi.org/10.1021/cm403039y | *Chem. Mater.* 2013, 25, 4378−4386

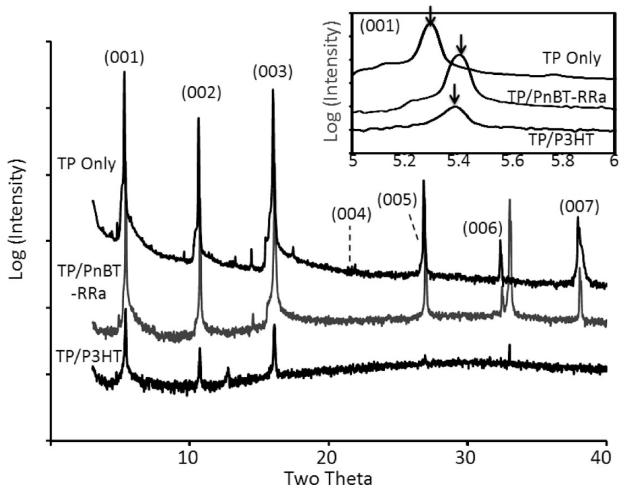

Figure 2. Grazing-incidence X-ray diffraction results for the three TP-based thin films. Notably, the pristine TP film has a (001) *d*-spacing of 1.669 nm, which is significantly larger than that of TP/PnBT-RRa (1.632 nm) and TP/P3HT blends (1.638 nm). The pristine TP films also have more non-(001) type reflections than the blended films.

spacings of the (001) peaks are 1.669, 1.638, and 1.632 nm, for pristine TP, TP/P3HT, and TP/PnBT-RRa, respectively. These results suggest that the needle- or wire-shaped crystals have (001) planes oriented parallel to substrate.[9,15] The long axis of the TP needles is previously designated as [210].[9,15] Although accurate peak intensity comparison in GIXRD requires accurate control of scan direction and symmetry, which is beyond the scope of this work, herein we qualitatively analyze film crystallinity based on Figure 2. (All films are fabricated under the same condition including concentration, drying rate, etc., so we assume their thickness values are comparable. This is further confirmed by the similar UV−vis peak intensities of TP absorption regions in different films (Figure S1b, Supporting Information). The dominating (001)-type reflections in all three TP-based films suggest preferred orientations along *c*-axis with (001) planes parallel to substrates in all cases. Therefore, herein we solely rely on the intensity of TP (001) planes for qualitative crystallinity analysis.) A pristine PnBT-RRa film is amorphous, evidenced by both GIXRD and SAED results, while P3HT films have a weak (001) peak at ∼1.600 nm, with a peak magnitude 5 times smaller than that of the TP/P3HT blend, and ∼100 times smaller than that of the TP/PnBT-RRa blend or pristine TP film (Figure S1a, Supporting Information). Figure S1a shows a comparison of the GIXRD peak intensities of TP/P3HT and TP/PnBT-RRa, which suggests that the (001)-type peak intensities of the TP/PnBT-RRa blend are generally more than 1 order of magnitude higher than those of TP/P3HT blend. Considering a crystallinity of pristine PnBT-RRa weaker than that of pristine P3HT, the higher (001) peak intensities and higher crystallinity of the TP/PnBT-RRa blend showcase the effect of structural similarity between the individual components (i.e., small molecule and polymer) and the participation of the TP component of the PnBT-RRa polymer in the resultant blend crystal structure. Stronger non-(001) type peaks appear in the pristine TP film, resulting from the needle-shaped crystals with a preferred orientation in film normal but random orientation in film plane.[18] On the other hand, the two blended films, especially the TP/PnBT-RRa film, show only a few non-(001) type peaks with low peak intensities, resulting from their improved grain orientation with well-defined 2D growth (Figure 2).

UV−vis absorption spectra of the blend films are compared in Figure S1b (Supporting Information), along with the spectra of pristine polymer and TP films. Although orientation dependent UV−vis absorption is not pursued in this study, efforts are made to compare the films in identical growth conditions, coverage areas, and orientation. The optical absorption of the pristine P3HT film demonstrates a characteristic, vibronic feature caused by the $\pi \rightarrow \pi^*$ transitions, with absorption maxima λ_{max}^{P3HT} of 606, 558, 519, and 481 nm, respectively, corresponding to 0−0, 0−1, 0−2, and 0−3 transition in solid state.[22] The pristine TP and PnBT-RRa films also show absorption maxima λ_{max}^{TP} (703, 651, 604, and 543 nm) and $\lambda_{max}^{PnBT\text{-}RRa}$ (693, 630, 580, and 534 nm) that agree with previously reported results.[20,23] Tables 1 and 2 compare the

Table 1. Measured UV-vis Absorption Shifts ($\Delta\lambda_{max}$) from the Absorption Maxima in Pristine Polymer (λ_{max}^{P3HT} in nm) or Small Molecule Film (λ_{max}^{TP} in nm) to the Ones in the TP/P3HT Blend ($\lambda_{max}^{TP/P3HT}$ in nm) Based on Spectra Shown in Figure S1b[a]

	peak shift from polymer to blend				peak shift from TP to blend		
	λ_{max}^{P3HT}	$\lambda_{max}^{TP/P3HT}$	$\Delta\lambda_{max}^{P3HT}$		λ_{max}^{TP}	$\lambda_{max}^{TP/P3HT}$	$\Delta\lambda_{max}^{TP}$
0−0	606	605	−1	0−0	703	701	−2
0−1	558	560	2	0−1	651	N/A	N/A
0−2	519	522	3	0−2	604	605	1
0−3	481	N/A	N/A	0−3	543	N/A	N/A

[a]A positive shift is a red shift, and a negative shift is a blue shift. There are a few $\lambda_{max}^{TP/P3HT}$ values (and corresponding shifts) labeled with "N/A" in the table, because of weak peak intensities or large overlaps with other stronger peaks. A typical measuring uncertainty is ±2 nm.

shifts in UV−vis absorption maxima ($\Delta\lambda_{max}$) from spectra of neat polymer (λ_{max}^{P3HT} and $\lambda_{max}^{PnBT\text{-}RRa}$) or small molecule film (λ_{max}^{TP}) to those observed in the blended films ($\lambda_{max}^{TP/P3HT}$ and $\lambda_{max}^{TP/PnBT\text{-}RRa}$). In general, the spectra for the TP/PnBT-RRa films show much larger peak shifts (up to 17 nm) compared to their TP/P3HT counterparts (≤3 nm). The magnitude of the shifts can be reasonably attributed to the structural similarity between the individual components and associated intermolecular interactions. More specifically, we expect that in the TP/P3HT blend, the $\pi-\pi$ interactions between the conjugated polymer and TP as well as the hydrophobic interactions between the polymer side chains and the triisopropylsilylethynyl side groups of TP are likely to contribute to the relatively small $\Delta\lambda_{max}$ values observed. On the other hand, in the TP/PnBT-RRa blend, the $\pi-\pi$ interactions between the acene backbones of PnBT-RRa and TP are expected to be much stronger than the interactions between the thiophenes of P3HT and acene backbone of TP because of an increased $\pi-\pi$ overlapping area, and the hydrophobic interactions in the TP/PnBT-RRa blend may also be much larger than those in the TP/P3HT blend because there are additional interactions between triisopropylsilylethynyl side groups of TP and PnBT, besides the interactions between triisopropylsilylethynyl side groups of TP and dodecyl groups of PnBT. Therefore, the much larger $\Delta\lambda_{max}$ values observed in the TP/PnBT-RRa blend are attributed to these largely increased intermolecular interactions.

dx.doi.org/10.1021/cm403039y | *Chem. Mater.* 2013, 25, 4378−4386

Table 2. Measured UV-vis Absorption Shifts ($\Delta\lambda_{max}$) from the Absorption Maxima in Pristine Polymer ($\Delta\lambda_{max}^{PnBT\text{-}RRa}$ in nm) or Small Molecule Film (λ_{max}^{TP} in nm) to the Ones in the TP/PnBT-RRa Blend ($\lambda_{max}^{TP/PnBT\text{-}RRa}$ in nm) Based on Spectra Shown in Figure S1b[a]

	peak shift from polymer to blend				peak shift from TP to blend		
	$\lambda_{max}^{PnBT\text{-}RRa}$	$\lambda_{max}^{TP/PnBT\text{-}RRa}$	$\Delta\lambda_{max}^{PnBT\text{-}RRa}$		λ_{max}^{TP}	$\lambda_{max}^{TP/PnBT\text{-}RRa}$	$\Delta\lambda_{max}^{TP}$
0−0	693	699	6	0−0	703	699	−4
0−1	630	647	17	0−1	651	647	−4
0−2	580	594	14	0−2	604	594	−10
0−3	534	538	4	0−3	543	538	−5

[a]A typical measuring uncertainty is ±2 nm.

Crystalline orientation and anisotropy play a vital role in our experiments and analysis. GIXRD measurements reported in this work are sensitive to electron density variations along a line parallel to the unit cell *c*-axis. To shed light on the spatial distribution of individual components in the blends, energy-filtered TEM images were collected for films slowly crystallized on TEM grids. Figure 3a shows overlays of a 0 eV image and sulfur map for TP/PnBT-RRa and TP/P3HT, respectively. In the grayscale 0 eV images, the TP crystals are darker because of high crystallinity (as suggested by the GIXRD results) and high electron density, while the sulfur maps, which are obtained with a standard three-window method to remove the background effect, are false-colored in red to show the polymer-rich regions. The coexistence of conjugated polymer and TP is confirmed in both blends, whereas there are distinct polymer-rich (Figure S2, Supporting Information) and small-molecule-rich regions in the TP/P3HT films (Figure S3, Supporting Information). From the sulfur map intensity scans on individual TP crystals along their long axis (Figure 3b), it is clear that TP crystals in TP/P3HT blends have distinctive sulfur-rich and sulfur-deficient regions, while TP crystals in TP/PnBT RRa blends generally have consistent and high sulfur content. The gaps between crystals represent much thinner areas with significantly less materials, which are outside the scope of our comparison. The TP/PnBT-RRa films generally show much more intimate mixing between the polymer and small molecule component, which again can be attributed to its high degree of structural similarity between individual components (i.e., small molecule semiconductor and conjugated polymer additive).

Figure 3c and 3d shows typical selected area electron diffraction patterns of TP/PnBT-RRa and TP/P3HT films, both in the [001] zone. On the basis of our GIXRD and [001] zone electron diffraction patterns, we use the triclinic unit cell of a_o = 0.755 nm, b_o = 0.773 nm, c_o = 1.702 nm, α_o = 89.5°, β_o = 78.7°, and γ_o = 81.0° (a_o/b_o = 0.98) to describe the pristine TP thin films slowly crystallized from dilute toluene solution. (The number of significant digits is chosen based on experimental uncertainties.) This unit cell, namely phase I, is almost identical to the reported unit cells for bulk and thermally evaporated films.[7,24,25] A 3 × 3 unit cell view of pristine TP bulk (phase I) crystal down the "*c*" axis is given in Figure S4 (Supporting Information) along with the corresponding simulated electron diffraction pattern ([001] zone), in which six reflections ($0\bar{2}0$), ($2\bar{2}0$), (200) (020), ($\bar{2}20$), and ($\bar{2}00$) are highlighted by yellow circles. These six reflections are used to monitor changes in the dimensions of the unit cell and to index the patterns of other TP polymorphs represented in Figure 3c,d. The [001] zone of TP/PnBT-RRa blends (Figure 3c) yields a_1 = 0.788 ± 0.004 nm, b_1 = 0.767 ± 0.007 nm, a_1/b_1 = 1.03, and γ_1 = 81 ± 1°, based on four to six measurements of each parameters. In contrast, the [001] zone of TP/P3HT

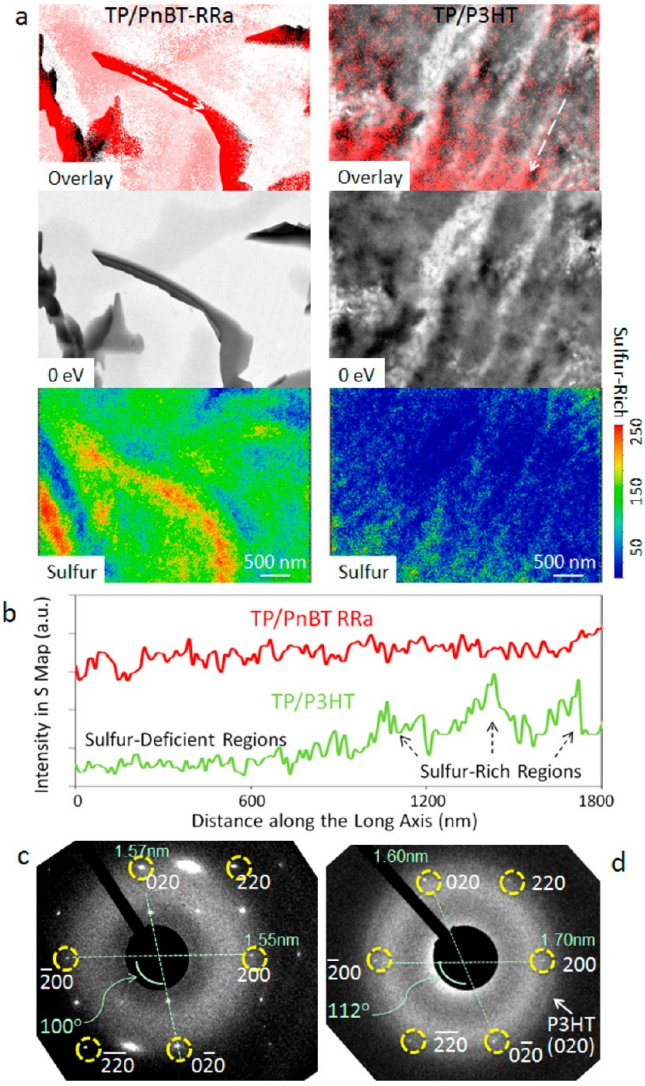

Figure 3. Overlays of the sulfur map (in red) and 0 eV image (in grayscale) show that the TP/PnBT-RRa blend has more intimate mixing than that of the TP/P3HT blend (a), which is further supported by the sulfur map intensity scans on individual TP crystals along their long axis (b). The position and direction of each scan are indicated in the overlay images with white, dashed arrows. (The raw images are shown along with the overlays.) The indexed [001] zone electron diffraction pattern of the TP/PnBT-RRa blend (c) has distinctively different *d*-spacings and γ angle, compared to that of the TP/P3HT blend (d). The proposed indexing of panels c and d is based on GIXRD results which suggest that (001) planes are oriented parallel to substrates and that the top-view SAED patterns presented here prevail throughout the *a*−*b* plane (i.e., [001] zone).

dx.doi.org/10.1021/cm403039y | *Chem. Mater.* 2013, 25, 4378−4386

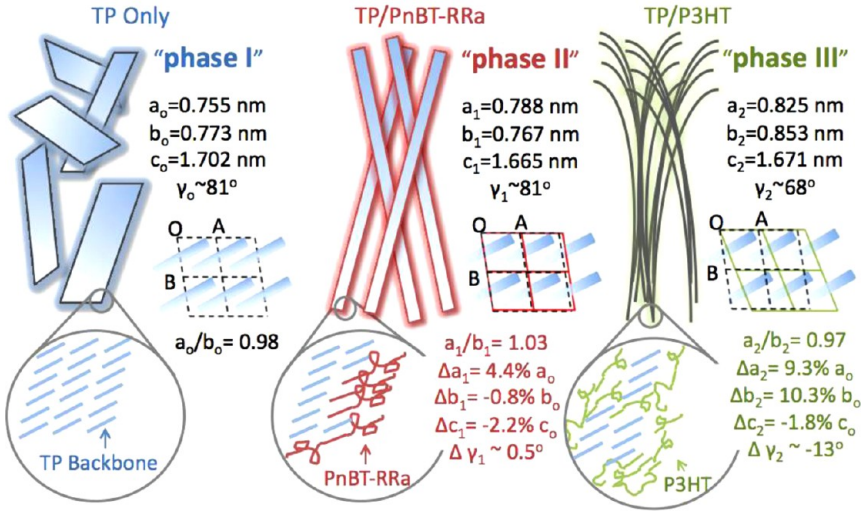

Figure 4. Drawings that compare film structure and unit cell parameters of the three TP-based films resulting from slow solution crystallization and blending with conjugated polymers. The needle- or wire-shaped TP crystals have (001) planes parallel to substrate, and the long axis of the TP crystals is previously assigned to [210].[9,15] The proposed unit cells for phases II and III are based on the GIXRD results that (001) planes preferably oriented parallel to substrates and the planar view SAED patterns in Figure 3c and 3d that consistently appear in the $a-b$ plane (suggesting a [001] zone).

blends (Figure 3d) gives a_2 = 0.825 ± 0.007 nm, b_2 = 0.853 ± 0.003 nm, a_2/b_2 = 0.97, and γ_2 = 68 ± 1°. Because the measured $d_{(001)}$ values from GIXRD are 1.669, 1.632, and 1.638 nm, for pristine TP, TP/PnBT-RRa, and TP/P3HT blend, respectively (Figure 2a) we estimate their c values to be c_o = 1.702 nm, c_1 = 1.665 nm, c_2 = 1.671 nm, given that α = ~90° and β is constant (β_o = 78.7°, sin 78.7° = 0.98, and even if β changes slightly, sin β ~ 1). As compared to the phase I structure of TP (a_o = 0.755 nm, b_o = 0.773 nm, a_o/b_o = 0.98, c_o = 1.702, and γ_o = 81.0°), the TP unit cell structure in the 1:1 (by weight) TP/PnBT-RRa blend (a_1 = 0.788 ± 0.004 nm, b_1 = 0.767 ± 0.007 nm, a_1/b_1 = 1.03, c_1 = 1.665 nm, and γ_1 = 81 ± 1°) has a nearly unchanged γ value, a larger "a" (4% larger than a_o), a smaller "b" and "c" (by 1% and 2%, respectively), and a reversed a/b ratio (0.98 versus 1.03). We name this previously unreported TP polymorph in TP/PnBT-RRa blends as phase II. On the other hand, comparison of phase I and the TP unit cell structure in the 1:1 (by weight) TP/P3HT blend (a_2 = 0.825 ± 0.007 nm, b_2 = 0.853 ± 0.003 nm, a_2/b_2 = 0.97, c_2 = 1.671 nm, and γ_2 = 68 ± 1°) shows that the unit cell of blend has a nearly unchanged a/b ratio, a slightly reduced c (by 2%), a considerably decreased γ (by 13°), and a largely increased a and b (by 9% and 10%, respectively). This new TP polymorph is named phase III. The cell volume (V) of phase II and III are calculated to be 974.3 Å^3 and 1066.3 Å^3, which are 1.3% and 10.9% larger than that of the phase I (V_o = 961.7 Å^3). The number of significant digits for cell volume is determined by following a previously published work.[6] The previously reported high temperature solution-processed thin film polymorph (above 124 °C) of TP (a_{HT} = 0.780 nm, b_{HT} = 0.720 nm, a_{HT}/b_{HT} = 1.08, c_{HT} = 1.720 nm, α_{HT} = 90.0°, β_{HT} =85.0°, and γ_{HT} = 88.0°)[24] has a calculated cell volume of 961.7 Å^3, identical to that of the phase I, whereas the solution sheared TP polymorphs generally have increasing cell volumes (991.1–1013.5 Å^3) as the solution shear speed is increased to an optimized value (0.4–2.8 mm/s) and the TP polymorph with the largest volume change corresponding to a significantly reduced $\pi-\pi$ stacking distance and the highest measured hole mobility.[6] Here we show that by simply using conjugated polymer additives in slow solution crystallization, the estimated cell volume could be significantly (>5%) larger than those achieved by the solution shearing method. In addition, unlike the case with solution shearing,[6] the cell volume change observed in this study is not introduced by external forces, but rather by conjugated polymer additives, which manifest in the UV–vis peak shifts (Table 1, and Figure S1b, Supporting Information). The larger cell volume of phases II and III as compared to phase I also indicates that the packing efficiencies in phases II and III are lower and the structures are metastable. This is similar to the case with the structures produced by the solution shearing method.[6] Additional representative electron diffraction patterns obtained from different locations of TP/PnBT-RRa films and the TP-rich regions of TP/P3HT films are shown in Figure S5 (Supporting Information), and these are in agreement with the patterns shown in Figure 3. It is necessary to point out that the indexing in Figure 3c and 3d is based on the facts that GIXRD measures electron density variations along a line parallel to the unit cell c-axis and that the top-view SAED patterns presented here prevail and consistently appear throughout the $a-b$ plane (i.e., [001] zone). The six circled reflections are chosen because they represent the main framework of the SAED patterns. The weaker reflection intensities in Figure 3d are caused by the lower crystallinity of TP/P3HT blends as evidenced by GIXRD results discussed previously. Also because of their lower crystallinity, not all reflections of the TP [001] zone are visible in TP/P3HT blends (Figure 3d).

Water contact angle measurements were used to gather information about the top surfaces of the blend films, which yielded a value of 75 ± 17° for TP/P3HT films and 97 ± 8° for TP/PnBT-RRa films. (Results, shown in Figure S6 (Supporting Information), are based on approximately five measurements for each film.) These results agree with the observation that the TP/P3HT films have more distinctive polymer-rich and TP-rich domains, as well as more uncovered surfaces, that lead to variations in the measurements compared to the TP/PnBT-RRa films. Because the selected, well-covered areas of pristine TP films have water contact angles of 97 ± 4° and the dodecyl

dx.doi.org/10.1021/cm403039y | Chem. Mater. 2013, 25, 4378–4386

thiophene component of the PnBT-RRa polymer has a water contact angle >110 ° (water contact angles are 109.8 ± 2.4° for poly(3-octylthiophene), 106.5 ± 0.3° for P3HT, and 102.1 ± 0.7° for poly(3-butylthiophene)),[26] we expect that the top layer of the TP/PnBT-RRa film is rich in TP or the TP portion of the PnBT-RRa polymer.

The drawings shown in Figure 4 summarize our findings concerning conjugated polymer-mediated polymorphism of TP-based blend films after slow solution crystallization, which highlights proposed changes in TP unit cell parameters and long-range order as a result of tuned intermolecular interactions and structural similarity between individual components of the blends. It is important to point out that the lack of similarity in molecular structures between the conjugated polymer additive and small molecule semiconductor (such as the case in the TP/P3HT blend) leads to less intimate mixing with weaker intermolecular interactions (as indicated by the UV−vis absorption results), yielding a polymorph with larger cell parameter changes. On the other hand, a higher degree of structural similarity (such as the case in the TP/PnBT-RRa blend) leads to more intimate mixing with stronger intermolecular interactions (as indicated by larger UV−vis shifts), promoting a polymorph with small cell parameter changes. We attribute this observation to the hypothesis that initial aggregated cluster formation and kinetics of heterogeneous nucleation are crucial in polymorphism.[1,2,4] Therefore, as we mentioned previously in Introduction, the involved intermolecular interactions between the additive and the nuclei in forming (including $\pi-\pi$ and hydrophobic interactions between the conjugated polymer additive and small molecule organic semiconductor) can strongly affect the final polymorph. It is likely that, in the early stage of crystallization, the small intermolecular interactions in TP/P3HT blend guides the TP nuclei or aggregated clusters into a metastable unit cell structure with significantly changed cell parameters, which is energetically favored in the presence of P3HT and the available intermolecular interactions, while the strong intermolecular interactions in TP and the TP portion of the PnBT-RRa polymer in TP/PnBT-RRa blends significantly (but not completely) compensate for this effect and result in a more stable unit cell structure with smaller lattice parameter changes. In addition, because thin film structures are the main focus of this work, a confinement-induced effect can play a role, which is less dependent upon intermolecular interactions but rather on the crystalline habitats of the conjugated polymer template. Detailed differentiation of the confinement effect and intermolecular interaction effect is not pursued here. Nevertheless, our study suggests that TP/conjugated polymer blends lead to TP crystal structures and film morphologies that are not accessible by nonconjugated polymer additives and external field-induced alignment methods. External alignment methods such as solution shear generally enhance the orientation of the needle-shaped TP crystals, while nonconjugated polymer additives serve as a matrix to disperse the needle-shaped crystal or induce vertical phase separation based on their entropic or hydrophobic driving forces. The availability of the additional $\pi-\pi$ interactions in the TP/conjugated polymer blends interestingly offers new crystallization pathways, and we attribute the formation of the novel morphologies observed here to these interactions between the conjugated polymers and small molecules.

It is known that the measured charge mobilities in OTFTs are heavily dependent on many measurement and fabrication details including external alignment, channel dimension, surface treatment, electrode treatment, etc. As previously reported from our laboratories and elsewhere,[8−12] pure TP-based OTFTs demonstrate the highest hole mobilities, ~1 $cm^2\ V^{-1}\ s^{-1}$, with small channel sizes of W = 6−300 μm and L = 5−30 μm, when proper external alignment methods are in place (without solution shear), while TP-based OTFTs only show average hole mobilities of less than 0.05 $cm^2\ V^{-1}\ s^{-1}$ with larger channel sizes and insufficient external alignment because of limited long-range order and crystal anisotropy.[15,18,27] Here in the absence of external alignment, we use a very large channel size (W = 2000 μm and L = 100 μm; channel area 30−1000 times higher than those mentioned previously) and a simple phenyltrichlorosilane (PTS) surface treatment[6] to demonstrate the effect of long-range order in the TP/conjugated polymer blends under the same fabrication conditions (Table 3). With this large channel size and PTS treatment (~10 devices), the pristine TP devices have hole mobilities between 1.0×10^{-4} and 0.11 $cm^2\ V^{-1}\ s^{-1}$ (average mobility of 0.02 ± 0.04 $cm^2\ V^{-1}\ s^{-1}$), in the absence of external alignment (Figure 5). In contrast, under the same fabrication conditions (i.e., without external aligning), the TP/P3HT blend yields hole mobilities ranging from 0.02 to 0.39 $cm^2\ V^{-1}\ s^{-1}$ (average of 0.17 ± 0.15 $cm^2\ V^{-1}\ s^{-1}$) (Figure 6) while the TP/PnBT-RRa blend yields hole mobilities between 0.06 and 0.14 $cm^2\ V^{-1}\ s^{-1}$ (average of 0.12 ± 0.03 $cm^2\ V^{-1}\ s^{-1}$) (Figure 7). Typical TP/P3HT devices fabricated by solution crystallization in air only show on/off ratios of less than 10^3 with large threshold voltages (up to 18 V) (Figure 6), which is likely caused by the low air stability of P3HT. Solution crystallization in inert gas, on the other hand, yields a significantly improved on/off ratio (up to 5×10^4) and threshold voltage (~3 V) for TP/P3HT devices as shown in Figure S7, Supporting Information. The larger performance variation in TP/P3HT devices is attributed to the curvature of their grasslike microwire morphology, while the "woven" straight needle patterns in TP/PnBT-RRa leads to better long-range order with more consistent device performance in this OTFT layout with large channel dimension. Significantly, the pristine PnBT-RRa-based OTFTs only have hole mobilities below 10^{-4} $cm^2\ V^{-1}\ s^{-1}$ (data not shown), and neat P3HT-based OTFTs show mobilities of ≤0.1 $cm^2\ V^{-1}\ s^{-1}$.[28] The observed highest mobilities from the TP/PnBT-RRa and TP/P3HT blends (0.14 and 0.39 $cm^2\ V^{-1}\ s^{-1}$, respectively) are by far larger than those values, implying that the TP component is playing a much more important role in charge transport of the

Table 3. A Summary of OTFT Device Performance of TP and TP/Conjugated Polymer Films *with No External Alignment* (W = 2000 μm and L = 100 μm; average and standard deviation are obtained from ~10 devices in each case)[a]

	maximum mobility μ_{MAX} ($cm^2\ V^{-1}\ s^{-1}$)	average mobility μ_{AVG} ($cm^2\ V^{-1}\ s^{-1}$)	standard deviation ($cm^2\ V^{-1}\ s^{-1}$)
TP only (phase I)	0.11	0.02	0.04
TP/PnBT-RRa (phase II)	0.14	0.12	0.03
TP/P3HT (phase III)	0.39	0.17	0.15

[a]Typical output and transfer characteristics are given in Figures 5−7.

dx.doi.org/10.1021/cm403039y | Chem. Mater. 2013, 25, 4378−4386

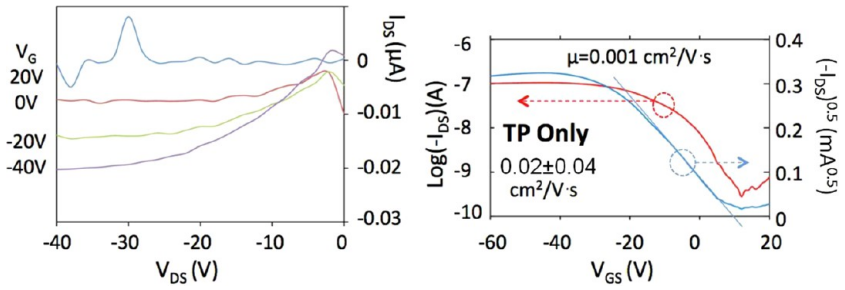

Figure 5. Typical output (left) and transfer characteristics (right) of top-contact, bottom-gate OTFTs based on pristine TP with a large channel size of W = 2000 μm and L = 100 μm *in the absence of external alignment*. For the transfer characteristics measurement, V_{DS} = −40 V.

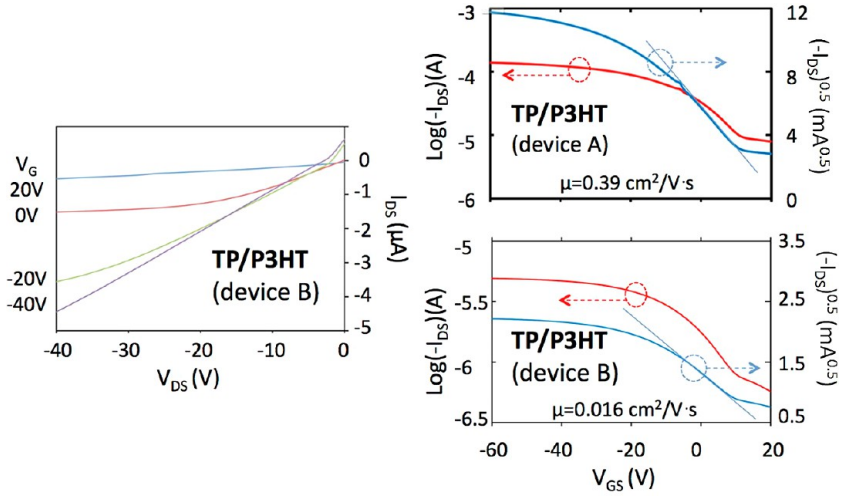

Figure 6. Representative output (left) and transfer characteristics (right) of OTFTs based on TP/P3HT blends with a large channel size of W = 2000 μm and L = 100 μm *in the absence of external alignment*, which have a large mobility fluctuation due to its curved "grasslike" microwire morphology. Device A is a typical device with higher mobility (0.390 cm^2 V^{-1} s^{-1}), and device B represents devices with significantly lower mobility (0.016 cm^2 V^{-1} s^{-1}).

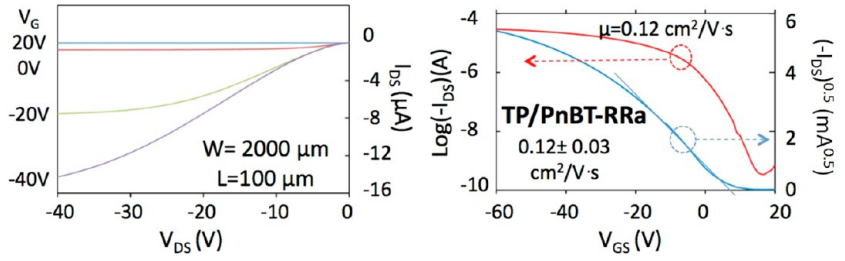

Figure 7. Representative output (left) and transfer characteristics (right) of OTFTs based on TP/PnBT-RRa blends with a large channel size of W = 2000 μm and L = 100 μm *in the absence of external alignment*.

TP/conjugated polymer blends than the intrinsic semiconducting behavior of the conjugated polymer additives. In other words, although the OTFT work performed here is based on bottom-gated devices and the bottom interface composition is largely unknown so far, the charge transport in TP domains is dominant in the TP/conjugated polymer blends, considering the relatively smaller motilities of conjugated polymer used. It is important to point out that because the long axis of TP crystals (i.e., [210]) represents a charge transport pathway with few grain boundaries[9,15] and TP (001) planes are parallel to substrates (according to GIXRD results), all reported mobility values are based on devices with most needle or wire structures vertically arranged to the channel width in this study. The improved performance in TP/conjugated polymer-based devices, however, cannot be solely attributed to polymorphism and unit cell changes. It is expected that the performance differences shown in Table 3 result from a combination of factors including long-range order, polymorphism, film coverage, and film morphology. The charge transport at grain boundaries could be a contributing factor, considering that TP/P3HT films have less sharp grain boundaries and more "eroded" ones. Further analyses of those individual effects are beyond the scope of this work.

■ CONCLUSION

In summary, we report a "conjugated polymer-mediated polymorphism" of a benchmark small molecule, organic semiconductor (TIPS pentacene or TP) in solution-crystallized thin films. This simple solution process provides a powerful way to manipulate the thin film structure and polymorphism of a

dx.doi.org/10.1021/cm403039y | *Chem. Mater.* 2013, 25, 4378−4386

small molecule organic semiconductor. In addition, it largely enhances the long-range order of the organic semiconductor thin film, which is potentially important for many organic electronic devices. The proposed approach explores tunable intermolecular interactions between the small molecule semiconductor and the conjugated polymer additives, yielding crystal structures that are not accessible by nonconjugated polymer additives and external field-induced alignment methods. We expect that the molecular weight, regioregularity, polydispersity, and the exact molecular structure of the conjugated polymer additives may all have an influence on structure−property relationships, along with other process conditions such as the polymer/small molecule ratio, solvent choice, rate of crystallization, crystallization temperature, substrate choice, and additional external alignment. The conjugated polymer-mediated polymorphism approach provides a new exciting avenue to explore correlations between crystal structure and charge transport in solution processed organic semiconductors, with this novel blending/cocrystallization approach introducing many unexplored processing parameters.

■ ASSOCIATED CONTENT

Supporting Information

Additional information as noted in the text. This material is available free of charge via the Internet at http://pubs.acs.org.

■ AUTHOR INFORMATION

Corresponding Authors

*E-mail: chenj1@ornl.gov.
*E-mail: zbao@stanford.edu.

Notes

The authors declare no competing financial interest.

■ ACKNOWLEDGMENTS

A portion of this research was conducted at the Center for Nanophase Materials Sciences, which is sponsored at Oak Ridge National Laboratory by the Scientific User Facilities Division, Office of Basic Energy Sciences, U.S. Department of Energy. D. Li acknowledges NSF support (EPS-1158862 and ECCS-1151140) and DOE Human Resource Development (HRD) travel fund (08-0217).

■ REFERENCES

(1) Bernstein, J. *Polymorphism in Molecular Crystals*; Oxford Univeristy Press: New York, 2002.
(2) Falini, G.; Albeck, S.; Weiner, S.; Addadi, L. *Science* **1996**, *271*, 67.
(3) Belcher, A. M.; Wu, X. H.; Christensen, R. J.; Hansma, P. K.; Stucky, G. D.; Morse, D. E. *Nature* **1996**, *381*, 56−58.
(4) (a) Price, C. P.; Grzesiak, A. L.; Matzger, A. J. *J. Am. Chem. Soc.* **2005**, *127*, 5512. (b) Lang, M. D.; Grzesiak, A. L.; Matzger, A. J. *J. Am. Chem. Soc.* **2002**, *124*, 14834.
(5) (a) Hermet, P.; Bantignies, J. L.; Rahmani, A.; Sauvajol, J. L.; Johnson, M. R. *J. Phys. Chem. A* **2005**, *109*, 4202−4207. (b) Mattheus, C. C.; Dros, A. B.; Baas, J.; Oostergetel, G. T.; Meetsma, A.; de Boer, J. L.; Palstra, T. T. M. *Synth. Met.* **2003**, *138*, 475. (c) Siegrist, T.; Kloc, C.; Schon, J. H.; Batlogg, B.; Haddon, R. C.; Berg, S.; Thomas, G. A. *Angew. Chem., Int. Ed.* **2001**, *40*, 1732. (d) Troisi, A.; Orlandi, G. *J. Phys. Chem. B* **2005**, *109*, 1849−1856. (e) Coropceanu, V.; Cornil, J.; da Silva, D. A.; Olivier, Y.; Silbey, R.; Bredas, J. L. *Chem. Rev.* **2007**, *107*, 926−952. (f) Fichou, D. *J. Mater. Chem.* **2000**, *10*, 571−588. (g) Campione, M.; Tavazzi, S.; Moret, M.; Porzio, W. *J. Appl. Phys.* **2007**, *101*, 6.
(6) Giri, G.; Verploegen, E.; Mannsfeld, S. C. B.; Atahan-Evrenk, S.; Kim, D. H.; Lee, S. Y.; Becerril, H. A.; Aspuru-Guzik, A.; Toney, M. F.; Bao, Z. *Nature* **2011**, *480*, 504.
(7) Anthony, J. E.; Brooks, J. S.; Eaton, D. L.; Parkin, S. R. *J. Am. Chem. Soc.* **2001**, *123*, 9482−9483.
(8) Park, S. K.; Jackson, T. N.; Anthony, J. E.; Mourey, D. A. *Appl. Phys. Lett.* **2007**, *91*, 063514.
(9) Chen, J.; Tee, C. K.; Shtein, M.; Anthony, J.; Martin, D. C. *J. Appl. Phys.* **2008**, *103*, 114513.
(10) Kang, J.; Shin, N.; Jang, D. Y.; Prabhu, V. M.; Yoon, D. Y. *J. Am. Chem. Soc.* **2008**, *130*, 12273.
(11) Kim, D. H.; Lee, D. Y.; Lee, H. S.; Lee, W. H.; Kim, Y. H.; Han, J. I.; Cho, K. *Adv. Funct. Mater.* **2007**, *19*, 678.
(12) Sakanoue, T.; Sirringhaus, H. *Nat. Mater.* **2010**, *9*, 736.
(13) Lee, W. H.; Kim, D. H.; Jang, Y.; Cho, J. H.; Hwang, M.; Park, Y. D.; Kim, Y. H.; Han, J. I.; Cho, K. *Appl. Phys. Lett.* **2007**, *90*, 3.
(14) Kim, M. J.; Heo, H. W.; Suh, Y. K.; Song, C. K. *Org. Electron.* **2011**, *12*, 1170.
(15) Chen, J.; Tee, C. K.; Shtein, M.; Martin, D. C.; Anthony, J. *Org. Electron.* **2009**, *10*, 696.
(16) Jung, H. J.; Shin, Y. J.; Park, Y. J.; Yoon, S. C.; Choi, D. H.; Park, C. *Adv. Funct. Mater.* **2010**, *20*, 2903.
(17) Hamilton, R.; Smith, J.; Ogier, S.; Heeney, M.; Anthony, J. E.; McCulloch, I.; Veres, J.; Bradley, D. D. C.; Anthopoulos, T. D. *Adv. Mater.* **2009**, *21*, 1166.
(18) He, Z.; Xiao, K.; Durant, W.; Hensley, D. K.; Anthony, J. E.; Hong, K.; Kilbey, S. M., II; Chen, J.; Li, D. *Adv. Funct. Mater.* **2011**, *21*, 3617.
(19) (a) Lada, M.; Starink, M. J.; Carrasco, M.; Chen, L. C.; Miskiewicz, P.; Brookes, P.; Obarowska, M.; Smith, D. C. *J. Mater. Chem.* **2011**, *21*, 11232−11238. (b) Li, X.; Kjellander, B. K. C.; Anthony, J. E.; Bastiaansen, C. W. M.; Broer, D. J.; Gelinck, G. H. *Adv. Funct. Mater.* **2009**, *19*, 3610.
(20) Jiang, Y.; Hong, S.; Oh, J. H.; Mondal, R.; Okamoto, T.; Verploegen, E.; Toney, M. F.; McGehee, M. D.; Bao, Z. N. *J. Mater. Chem.* **2012**, *22*, 4356−4363.
(21) Chen, J.; Martin, D. C.; Anthony, J. E. *J. Mater. Res.* **2007**, *22*, 1701.
(22) (a) Li, G.; Yao, Y.; Yang, H.; Shrotriya, V.; Yang, G.; Yang, Y. *Adv. Funct. Mater.* **2007**, *17*, 1636−1644. (b) Trznadel, M.; Pron, A.; Zagorska, M. *Macromolecules* **1998**, *31*, 5051.
(23) Davis, R. J.; Lloyd, M. T.; Ferreira, S. R.; Bruzek, M. J.; Watkins, S. E.; Lindell, L.; Sehati, P.; Fahlman, M.; Anthony, J. E.; Hsu, J. W. P. *J. Mater. Chem.* **2011**, *21*, 1721.
(24) Chen, J.; Anthony, J.; Martin, D. C. *J. Phys. Chem. B* **2006**, *110*, 7928.
(25) Mannsfeld, S. C. B.; Tang, M. L.; Bao, Z. *Adv. Mater.* **2011**, *23*, 127.
(26) Robinson, L.; Isaksson, J.; Robinson, N. D.; Berggren, M. *Surf. Sci.* **2006**, *600*, 148.
(27) Headrick, R. L.; Wo, S.; Sansoz, F.; Anthony, J. E. *Appl. Phys. Lett.* **2008**, *92*, 3.
(28) (a) Yu, X.; Xiao, K.; Chen, J.; Lavrik, N. V.; Hong, K.; Sumpter, B. G.; Geohegan, D. B. *ACS Nano* **2011**, *5*, 3559. (b) Sirringhaus, H.; Brown, P. J.; Friend, R. H.; Nielsen, M. M.; Bechgaard, K.; Langeveld-Voss, B. M. W.; Spiering, A. J. H.; Janssen, R. A. J.; Meijer, E. W.; Herwig, P.; de Leeuw, D. M. *Nature* **1999**, *401*, 685.